The contribution of Cr and Ni to hydrogen absorption energy in Fe-Cr-Ni austenitic systems: A first-principles study

Junichiro Moriyama[a], Osamu Takakuwa[b,c], Masatake Yamaguchi[d,e,f], Yuhei Ogawa[g], Kaneaki Tsuzaki[c,f,g,h]

[a] *Graduate School of Mechanical Engineering, Kyushu University, 744 Motooka, Nishi-ku, Fukuoka 819-0395, Japan*

[b] *Department of Mechanical Engineering, Kyushu University, 744 Motooka, Nishi-ku, Fukuoka 819-0395, Japan*

[c] *Research Center for Hydrogen Industrial Use and Storage (HYDROGENIUS), Kyushu University, 744 Motooka, Nishi-ku, Fukuoka 819-0395, Japan*

[d] *Center for Computational Science and e-Systems, Japan Atomic Energy Agency (JAEA), 2-4 Shirakata, Tokai-mura, Naka-gun, Ibaraki 319-1195, Japan*

[e] *Department of Materials Science and Engineering, The University of Tokyo, 7-3-1 Hongo, Bunkyo-ku, Tokyo 113-8656, Japan*

[f] *Elements Strategy Initiative for Structural Materials, Kyoto University, Yoshida-honmachi, Sakyo-ku, Kyoto 606-8501, Japan*

[g] *National Institute for Materials Science (NIMS), 1-2-1 Sengen, Tsukuba, Ibaraki 305-0047, Japan*

[h] *Professor emeritus, Kyushu University, 744 Motooka, Nishi-ku, Fukuoka 819-0395,*

Japan

Corresponding author: Junichiro Moriyama
E-mail: moriyama.junitiro.953@s.kyushu-u.ac.jp

Abstract

The present study focuses on a novel hydrogen-improved strength-ductility balance in several practical Fe-Cr-Ni-based austenitic alloys that directly depends on the dissolved hydrogen content. The hydrogen absorption energy of Fe-Cr-Ni model alloys that have a face-centered cubic structure was examined using first-principles calculations to verify the contribution of Cr and Ni substitutions from Fe to hydrogen solubility in these alloys. Chromium substitution reduced the hydrogen absorption energy to a substantially greater degree than does Ni substitution, with increased Cr : Ni ratios resulting in higher hydrogen solubility. This pattern seen in the calculations supports the previously obtained experimental results in practical alloys with various Cr : Ni ratios. The pronounced reduction in hydrogen absorption energy that results from Cr substitution was mostly attributed to a decrement in the chemical effect derived from the electronic binding state rather than a mechanical effect caused by changed interatomic spacing due to these substitutions. We propose here a Cr-equivalent index to predict hydrogen solubility in Fe-Cr-Ni-based alloys that have varying Cr and Ni content.

Keywords: Austenitic alloy; First-principles calculation; Hydrogen; Absorption energy; Occupancy

1. Introduction

Hydrogen (H) causes a deterioration in various mechanical properties of metallic materials: of ductility [1], strength [2], and fracture toughness [3]. This is the well-known phenomenon of hydrogen embrittlement (HE). Since HE is a barrier to the progress of using H as an energy carrier, a substantial number of studies have been conducted to understand the underlying mechanisms of HE. It is hoped that metals and alloys with higher resistance to HE can be developed by suppressing these multiple HE-

triggers.

Fe-Cr-Ni-based austenitic alloys with a face-centered cubic (FCC) structure have a higher resistance to HE than body-centered cubic (BCC) structure alloys such as carbon steels [4] and martensitic steels [5]. However, if the stability of the austenitic phase is low, the structural changes in crystals transforming from FCC to BCC make them susceptible to HE [6,7]. The susceptibility to HE of austenitic alloys has been represented by the Ni-equivalent, which is given by the sum of the relative contributions of alloying elements to the stability of the austenitic phase [8]. In 18 mass%Cr-8 mass%Ni-based austenitic stainless steel (18Cr-8Ni), which has a metastable FCC phase, HE appears as a reduction in ductility and crack propagation resistance [9], while 18Cr-12Ni and 24Cr-19Ni have superior resistance to HE owing to their high Ni-equivalent [9,10].

Dissolved H hardens some FCC metals and alloys, as seen in pure Ni [11,12], Cu-Ni alloy [13], and Fe-Cr-Ni-based austenitic alloys [14]. Dissolved H has also been shown to improve the ductility of Fe-Mn alloy [15] and high-entropy Fe-Mn-Ni-Cr-Co alloy [16]. These facts suggest that dissolved H can be used as a key alloying element to develop novel structural materials with better mechanical performance. Ogawa et al. revealed that, in 24Cr-19Ni, the higher the dissolved H content, the greater the improvement in the strength-ductility balance [17]. Mechanical improvements such as this in Fe-Cr-Ni-based austenitic alloys depend on Cr and Ni content: alloys with a higher Cr content and Cr : Ni ratio achieve higher dissolved H content, amplifying the positive impacts of H [18]. Notably, dissolved H has potential similar to that of carbon and nitrogen for solid-solution hardening in the austenitic phase [18]. Consequently, the interrelation between dissolved H content and Cr and Ni in Fe-Cr-Ni-based austenitic alloys needs to be rationalized on an atomic scale to make dissolved H more effective as a beneficial alloying element.

First-principles calculation based on density functional theory (DFT) is one of the most suitable ways to characterize the atomic-scale interaction between metals and solutes. Dissolved H content can be evaluated by the energy required to solidify H in a Fe-Cr-Ni atomic system, i.e., H-absorption energy. We can therefore derive a quantitative understanding of dissolved H content in Fe-Cr-Ni-based austenitic alloys by unveiling the contributions of the alloying elements (Cr, Ni) to the H-absorption energy.

It has been reported that the alloying elements and their magnetic states alter the H-absorption energy across Fe-Cr-Ni-based austenitic stainless steels (AISI304 and 316L), Co-Cr-Fe-Ni, and Co-Cr-Fe-Mn-Ni high entropy alloys [19]. In Fe-Mn [20,21] and Fe-Al [22] systems, replacing a Fe atom surrounding O-sites with Mn or Al decreases H-absorption energy. Although the contribution of certain alloying elements to the H-absorption energy remains a concern in HE-relevant research, no systematic studies have yet directly compared dissolved H content from experiments with those from the H-absorption energy in various Fe-Cr-Ni-based austenitic alloys.

In the present study, we aim to examine the contributions of Cr and Ni to the dissolved H content of Fe-Cr-Ni-based austenitic alloys based on a systematic calculation of the H-absorption energy at interstitial positions in the vicinity of Cr or Ni atoms using DFT calculations. The H-absorption energy was divided into elastic energy, caused by the movement of the solvent atoms invoked by dissolved H, and chemical energy, stemming from the change in electronic binding states, which makes it possible to identify the role of each alloying element in the H-absorption energy. The dissolved H content, i.e., H-occupancy, was calculated using the H-absorption energy while varying Cr and Ni content, and then compared to the experimental results.

2. Computational methodology

2.1 Calculation method

The DFT calculations were performed using the Vienna Ab Initio Simulation Package [23–25] within the generalized gradient approximation of the Perdew-Burke-Ernzerhof form for electron exchange and correlation [26]. The projector-augmented wave (PAW) method was used for plane wave expansion [27]. Fe-Cr-Ni atomic systems with FCC structure were simulated using a 2×2×2 supercell with 32 atoms ($Fe_{31}X_1$, $Fe_{30}X_2$(X: Fe, Cr, Ni)). For example, the system with two atoms replaced by Cr denotes $Fe_{30}Cr_2$. We calculated the H-absorption energy when Cr or Ni replaces one or two of the 32 Fe atoms using these supercells. It was also calculated for Cr_{32} and Ni_{32}, in which Cr or Ni replaces all the Fe atoms. The bulk properties were calculated using a sufficiently high plane-wave cutoff energy of 360 eV with Fermi surface smearing [28] to obtain accurate interatomic forces, employing a smearing width of 0.2 eV. A 6×6×6 k-point Monkhorst-Pack grid [29] was used. We employed VESTA (Visualization for

Electric and Structural Analysis) [30] to visualize the atomic structure.

2.2 DFT calculations of H-absorption energies in $Fe_{31}X_1$, $Fe_{30}X_2$ (X: Fe, Cr, Ni)

Both cell geometry and atomic positions were fully relaxed in the $Fe_{31}X_1$, and $Fe_{30}X_2$ (X: Fe, Cr, Ni) unit cells when calculating the H-absorption energy. The magnetic state should be considered, as it impacts the H-absorption energy, as reported by Zhou et al [19]. The atomic structure in the Fe-Cr-Ni-based austenitic alloy is stable over a finite temperature range when in a paramagnetic (PM) state; it is unstable at T = 0K. When assuming the PM state in the DFT calculation, the H-absorption energy should include excess energy to stabilize the magnetic state. Hence, the antiferromagnetic double layer (AFMD) state (Fig. 1 (a)), i.e., a stable state at T = 0K, is appropriate for investigating the H-absorption energy using the DFT calculation [31]. Even though a recent study revealed that a spin-spiral state is the most stable in Fe with an FCC structure at T = 0K [32], the total energy of the AFMD state is similar to the spin-spiral state [33]. In the present study we therefore employed the AFMD state for analyzing the H-absorption energy.

The initial magnetic moment of Fe, Cr, and Ni atoms is ± 3.00μ_B, ± 5.00μ_B, and ± 1.00μ_B, where positive and negative values respectively mean up- and down-spin. After the calculations, the value of the magnetic moment within the PAW sphere of Fe, Cr, and Ni atoms changed to ± 2.03μ_B, ± 0.230μ_B, and ± 0.950μ_B, closely consistent with the results of previous studies [19,34]. The H-absorption energy in the non-magnetic (NM) state (Fig. 1 (b)) was also calculated. The H-absorption energy E_{ab} is given by:

$$E_{ab} = E_{tot}[Fe_{32-n}X_nH_1] - E_{tot}[Fe_{32-n}X_n] - \frac{1}{2}E_{tot}[H_2] + E_{ZP} \quad (1)$$

$E_{tot}[Fe_{32-n}X_nH_1]$, $E_{tot}[Fe_{32-n}X_n]$, and $E_{tot}[H_2]$ were total energy of $Fe_{32-n}X_nH_1$, $Fe_{32-n}X_n$, and H_2 molecule. The part of zero-point energy E_{ZP}, of H atom is given by:

$$E_{ZP} = \frac{1}{2}h\nu - ZPE[1/2\,H_2] \quad (2)$$

h, ν denote the Plank constant, and the vibrational frequency of the H atom in $Fe_{32-n}X_nH_1$, respectively. The $ZPE[1/2\,H_2]$ is half the zero-point energy of the H_2 molecules. The vibrational frequency was calculated throuth harmonic approximation. The hessian of the vibration of the H atom was obtained with the location of the other

fixed atom to decouple the vibration of the H atom from that of the other atom.

2.3 Deviation of elastic and chemical energy in the H-absorption energy

The H-absorption energy can be divided into elastic and chemical parts. The elastic part stems from the movement of the solvent atoms invoked by dissolved H, and the chemical part stems from changes in electronic binding state. Each was separately defined as "elastic energy", E_{ab}^{ela}, and "chemical energy", E_{ab}^{chem}, in the H-absorption energy, E_{ab}. The E_{ab}^{ela} and E_{ab}^{chem} are given by

$$E_{ab}^{ela}=E_{tot}^{pulloutH}[Fe_{32-n}X_n]-E_{tot}[Fe_{32-n}X_n] \quad (3)$$

$$E_{ab}^{chem}=E_{ab}-E_{ab}^{ela}-E_{ZP} \quad (4)$$

$E_{tot}^{pulloutH}[Fe_{32-n}X_2]$ is the total energy of $Fe_{32-n}X_n$ unit cell comes from removing the H atom from fully relaxed $Fe_{32-n}X_nH_1$.

2.4 DFT calculations of the H-absorption energy in Cr_{32} and Ni_{32} systems

More precisely, the H-absorption energy in pure Fe, Cr, and Ni systems should be resolved to estimate the intrinsic effect of Cr and Ni on the H-absorption energy. The H-absorption energy in Fe and Ni with FCC structure at absolute zero was estimated by extrapolation from the experimental data obtained at high temperatures [35]. Since the Cr element only shows a BCC structure in a solid state over the conventional temperature range, a Cr_{32} system with an FCC structure was hypothetically constructed. The ferromagnetic (FM) state (Fig. 1 (c)) for the Ni_{32} system with the initial magnetic moment was $1.00\mu_B$. Both cell geometry and atomic positions were fully relaxed in the unit cell. As a result, the magnetic moment changed to $0.642\mu_B$ (within the PAW sphere) a value that is consistent with a past study that gave a value of $0.641\mu_B$[36]. The magnetic state (AFMD), antiferromagnetic single layer (AFMS) state (Fig. 1 (d)), and nonmagnetic (NM) state were employed for the Cr_{32} systems with an initial magnetic moment of $\pm 5.00\mu_B$. As a result, in all magnetic states of Cr_{32} systems, the magnetic moment changed to $0.00\mu_B$ (within the PAW sphere) a value that is consistent with a past study that gave $0.00\mu_B$ [36].

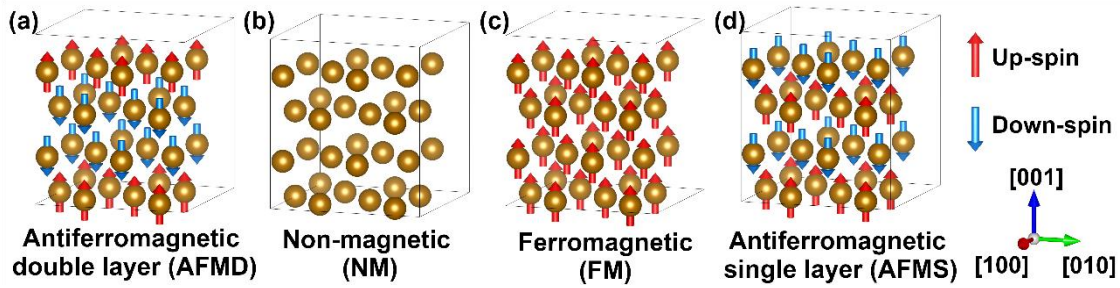

Fig. 1. The magnetic state of the unit cell with 32 atoms. (a) Antiferromagnetic double layer (AFMD), (b) Non-magnetic (NM), (c) Ferromagnetic (FM), and (d) Antiferromagnetic single layer (AFMS) state. The up and down arrows in AFMD, FM, and AFMS represent up- and down-spin.

2.5 Calculation of H occupancy

H-occupancy, θ_{L}, describes the dissolved H content, which represents the ratio of the internal sites occupied by the H atom, given by the following equation:

$$\theta_{\mathrm{L}}=\frac{1}{1+\exp\left(\frac{E_{\mathrm{ab}}-\mu^{*}}{k_{\mathrm{B}}T}\right)} \tag{5}$$

$$\mu^{*}=-\frac{7}{4}k_{\mathrm{B}}T\ln\frac{T}{T^{*}}+\frac{1}{2}k_{B}T\ln\frac{f}{f_{0}} \tag{6}$$

$$f=p\exp\left(\frac{pV_{H}}{RT}\right) \tag{7}$$

The chemical potential of the H atom, μ^{*}, can be calculated using Eq. (6). k_{B} is the Boltzmann constant and T is the temperature. T^{*} is the reference temperature of 7.55 K [35], and f denotes the fugacity of H_2 gas given by Eq. (7) with the gas pressure, p, the gas constant R $(=8.31\ J/(K\cdot mol))$, the molar volume of H_2, V_H $(=1.584\times10^{-5}\ \mathrm{m^3/mol})$ [37], and the reference fugacity, f_0 $(=0.1\mathrm{MPa})$. We calculated the H-occupancy with $p=100$ MPa at $T=543$ K for comparison with the experimental data obtained by the authors [18,38]. The method of calculating the H-occupancy using H-absorption energy will be described in Section 4.2.

3. H-absorption energy of $Fe_{31}X_1$, $Fe_{30}X_2$ in the Fe-Cr-Ni atomic system

3.1 Validity of computational settings

Convergence tests were performed to validate the calculation conditions in the present study using a unit cell size of 32 atoms, K-point of 6×6×6, and cutoff energy of

360 eV. When changing the unit cell size to four, 32, and 108 atoms in an NM state, the H-absorption energy was 0.145 eV for four atoms, 0.0662 eV for 32 atoms, and 0.0820 eV for 108 atoms. A unit cell with 32 atoms was therefore employed to acquire accurate H-absorption energy, taking into account calculation costs. Figure 1 shows the H-absorption energy obtained by the convergence test by varying K-point and cutoff energy in the unit cell consisting of 32 Fe atoms without a zero-point energy correction. The H-absorption energy is equivalent in the order of 10^{-1} eV regardless of the K-point and cutoff energy, similar to past studies giving 0.09 eV (Nazarov et al.) [34], and 0.13 eV (Ismer et al.) [20]. The unit cell size of 32 atoms with a K-point of 6×6×6, and the cutoff energy of 360 eV therefore ensures the accuracy of this study in investigating the effects of Cr and Ni solute atoms with various configurations.

Table 1. H-absorption energy of the unit cell consisting of 32 atoms with various K-point and cutoff energy without the zero-point energy correction

Condition	**K-point**	**cutoff energy (eV)**	**H-absorption energy (eV)**
Employed conditions	6×6×6	360	0.132
K-point (1)	7×7×7	360	0.138
K-point (2)	8×8×8	360	0.139
K-point (3)	9×9×9	360	0.138
cutoff energy (1)	6×6×6	400	0.132
cutoff energy (2)	6×6×6	500	0.123
cutoff energy (3)	6×6×6	600	0.122

3.2 H-absorption energy at O-sites and T-sites

Figures 2 and 3 show the H-absorption energy E_{ab} in the O-sites and T-sites, respectively, when replacing one Fe atom, i.e., $Fe_{31}X_1$, as represented in (a) or two Fe atoms, i.e., $Fe_{30}X_2$, as shown in (b). The part of the zero-point energy correction, E_{ZP}, is shown as bars filled with a hatched pattern. The up and down arrows in the figures denote the magnetic moment as up- and down-spin. The E_{ab} fell to a minimum at 0.118 eV for $Fe_{31}Cr_1$ and to 0.125 eV for $Fe_{31}Ni_1$, and 0.0490 eV for $Fe_{30}Cr_2$ and 0.0961 eV for $Fe_{30}Ni_2$. E_{ab} represents the stability of the H atom, since the lower the energy, the

more stable the site. The H atom can remain more stable in the Fe-Cr system than in the Fe-Ni system. The O-sites have a noticeably lower E_{ab} than the T-sites, regardless of the substituted element (Cr or Ni), for both $Fe_{31}X_1$ and $Fe_{30}X_2$, except when two Ni atoms are placed diagonally in $Fe_{30}Ni_2$ (type 2-2 and 3-2 in Fig. 3 (b)). In 2-2 and 3-2 in Fig. 3 (b), the structure relaxation invoked the extensive movement of atoms, i.e., change in the lattice constant, substantially affecting the H-absorption energy. As reported in past studies, the O-sites work as a solution site for H atoms [39] and the T-sites act as a diffusion pathway [20], i.e., the saddle point of activation energy. In the present study, therefore, we focus on E_{ab} at the O-sites in our calculations.

The following: 1) magnetic state, 2) location of substitutional atoms, and 3) number of substitutional atoms are dominant factors that control the H-absorption energy, E_{ab}. In 1) magnetic state, AFMD decreased the E_{ab} by replacing Fe with Ni and Cr, and Cr decreased it in the NM state. In 2) location of substitutional atoms, when replacing Fe with Ni, E_{ab} changed as a function of the location of Ni. However, the location of Cr did not influence E_{ab}. Cr and Ni thus appear to contribute in different ways to the reduction of E_{ab}. The insights from 1) and 2) indicate that E_{ab} is strongly affected by magnetic moments but not by their direction (up or down). In 3) number of substitutional atoms, one-atom substitution invoked the reduction in E_{ab} of 0.0614 eV by Ni and 0.068 eV by Cr, which became more pronounced in two-atom substitution, to 0.0901 eV by Ni and 0.130 eV by Cr. Chromium therefore plays a more influential role than Ni in reducing E_{ab}. This conclusion corresponds to the experimental results, which show that the higher the Cr content, or the higher the Cr : Ni ratio, the higher the dissolved H content in Fe-Cr-Ni-based austenitic alloys [18].

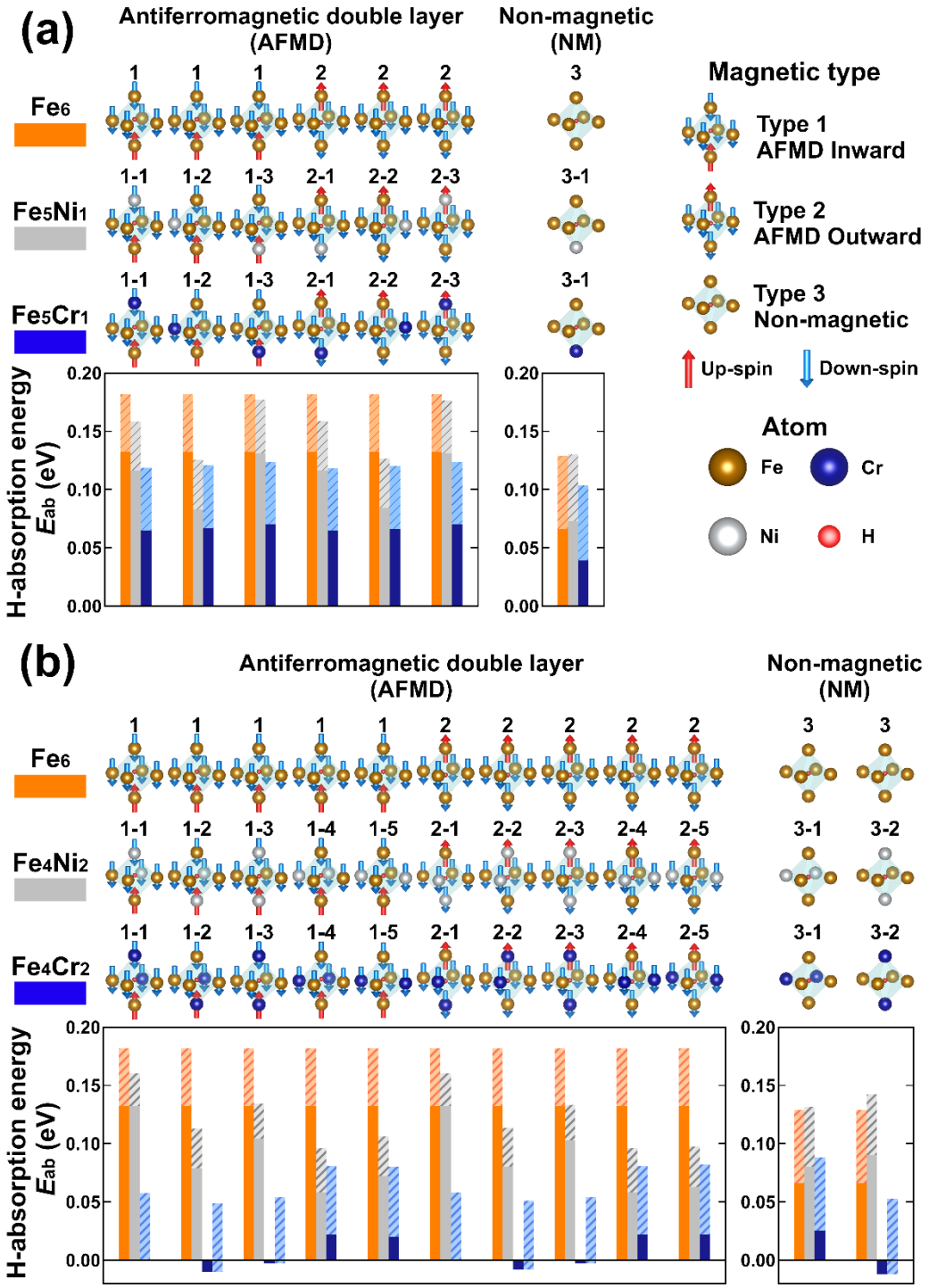

258 **Fig. 2**. H-absorption energy, E_{ab}, at the O-sites of (a) $Fe_{31}X_1$ and (b) $Fe_{30}X_2$ (X: Fe, Ni, Cr) in the AFMD
259 and NM states. Up and down arrows in the AFMD state represents the up- and down-spin. The part of
260 zero-point energy correction, E_{ZP}, is shown as bars filled with a hatched pattern.
261

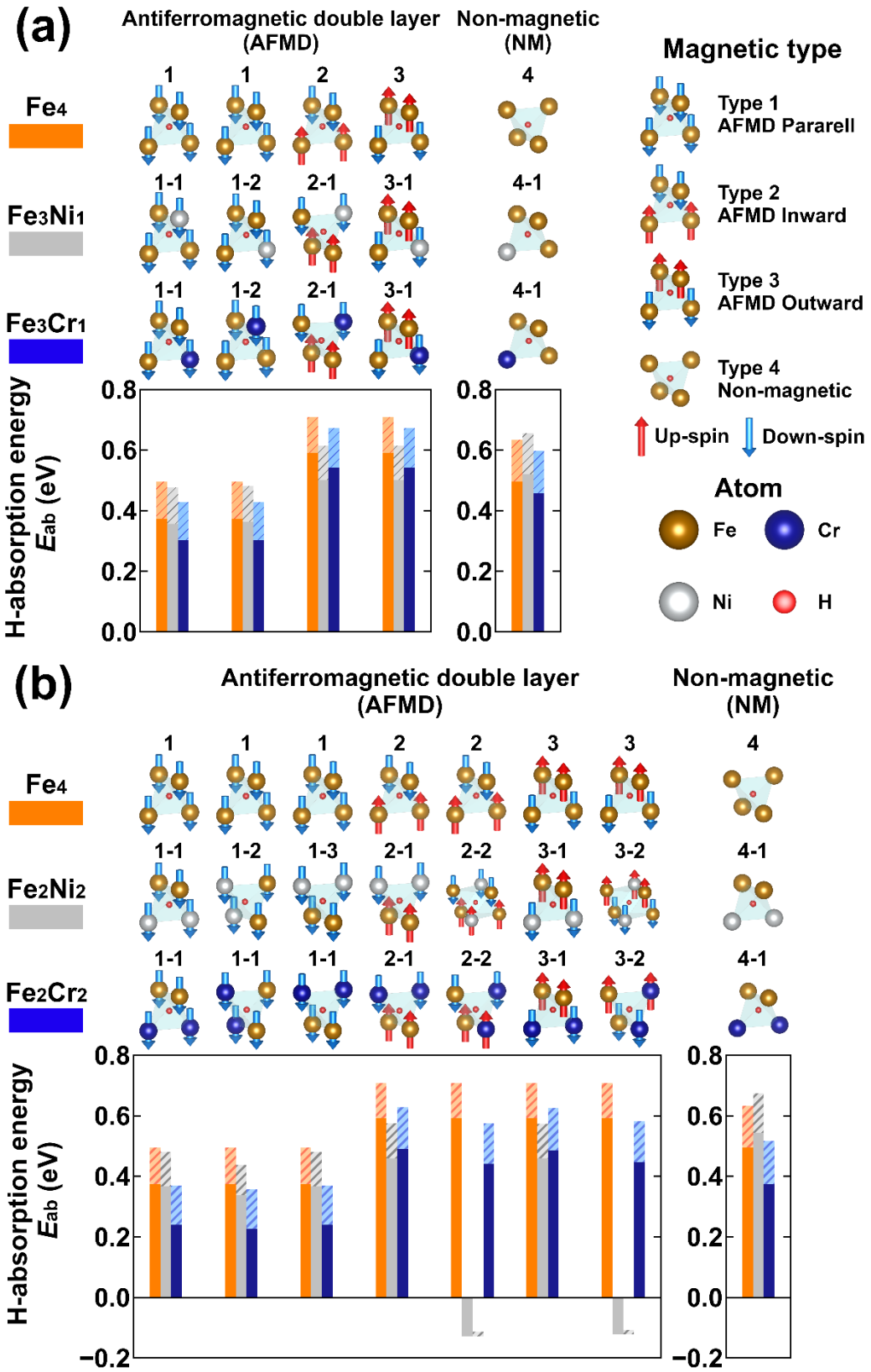

Fig. 3. H-absorption energy, E_{ab}, at the T-sites of (a) $Fe_{31}X_1$ and (b) $Fe_{30}X_2$ (X: Fe, Ni, Cr) in the AFMD and NM states. Up and down arrows in the AFMD state represent the up- and down-

spin. The part of zero-point energy correction, E_{ZP}, is shown as bars filled with a hatched pattern. The values of 2-2 and 3-2 of Fe_2Ni_2 in (b) did not represent correct H-absorption energy at the T-sites because of the significant movement of the H atoms and the change in the lattice constant of the unit cell during the structure relaxation calculation.

3.3 Contribution of elastic and chemical energy to H-absorption energy

Figures 4 and 5 respectively show elastic energy, E_{ab}^{ela}, and chemical energy, E_{ab}^{chem}, in (a) $Fe_{31}X_1$ and (b) $Fe_{30}X_2$ systems. Ni-substitution increased or decreased E_{ab}^{ela} depending on their positions, e.g., 0.0690 eV and 0.0793 eV in $Fe_{31}Ni_1$ as represented in type 1-1 and 1-3 in Fig. 4 (a). Cr-substitutions increased E_{ab}^{ela} in all cases (Fig. 4). In contrast, both Ni- and Cr-substitution decreased E_{ab}^{chem} in all cases (Fig. 5). Interestingly, the effect on E_{ab}^{chem} became more pronounced as the number of substituted atoms increased, irrespective of magnetic moment, especially for Cr-substitutions, where E_{ab}^{chem} became negative, e.g., –0.0164 eV in $Fe_{31}Cr_1$. The reduction in total H-absorption energy therefore stems from a marked decrease in the chemical energy part owing to the change in the electronic state, which is more pronounced in the Cr-substitutions.

To more precisely demonstrate the contribution of Cr and Ni to the reduction in the H-absorption energy, Fig. 6 shows the H-absorption energy, E_{ab}, in (a), the elastic energy, E_{ab}^{ela}, in (b), and the chemical energy, E_{ab}^{chem}, in (c) when Cr and Ni replace all Fe atoms in the unit cell. The part of zero-point energy correction, E_{ZP}, is represented as bars filled with a hatched pattern in (a). Due to Cr-substitutions, E_{ab}^{ela} showed a slight increase during the remarkable reductions in E_{ab}^{chem}, i.e., –0.321 eV from Fe_5Cr_1 to Cr_6. The reduction in E_{ab}^{chem} was independent of magnetic state because it transformed from AFMD and AFMS to NM during the structure relaxation. In contrast, E_{ab}^{chem} did not change with Ni-substitution, while a slight reduction emerged in E_{ab}^{ela} (–0.0192 eV, attributable to the change in the magnetic state, AFMD, and FM): Cr reduces E_{ab} by potentially lowering E_{ab}^{chem}, and Ni by E_{ab}^{ela}. Cr-substitution is more effective in reducing E_{ab}. The experimental values of the H-absorption energy for Fe with an FCC structure and Ni are positive, at 26.2 and 14.6 kJ/mol [35]. Chromium, therefore, as demonstrated by the present study, contributes more to reducing the H-absorption energy.

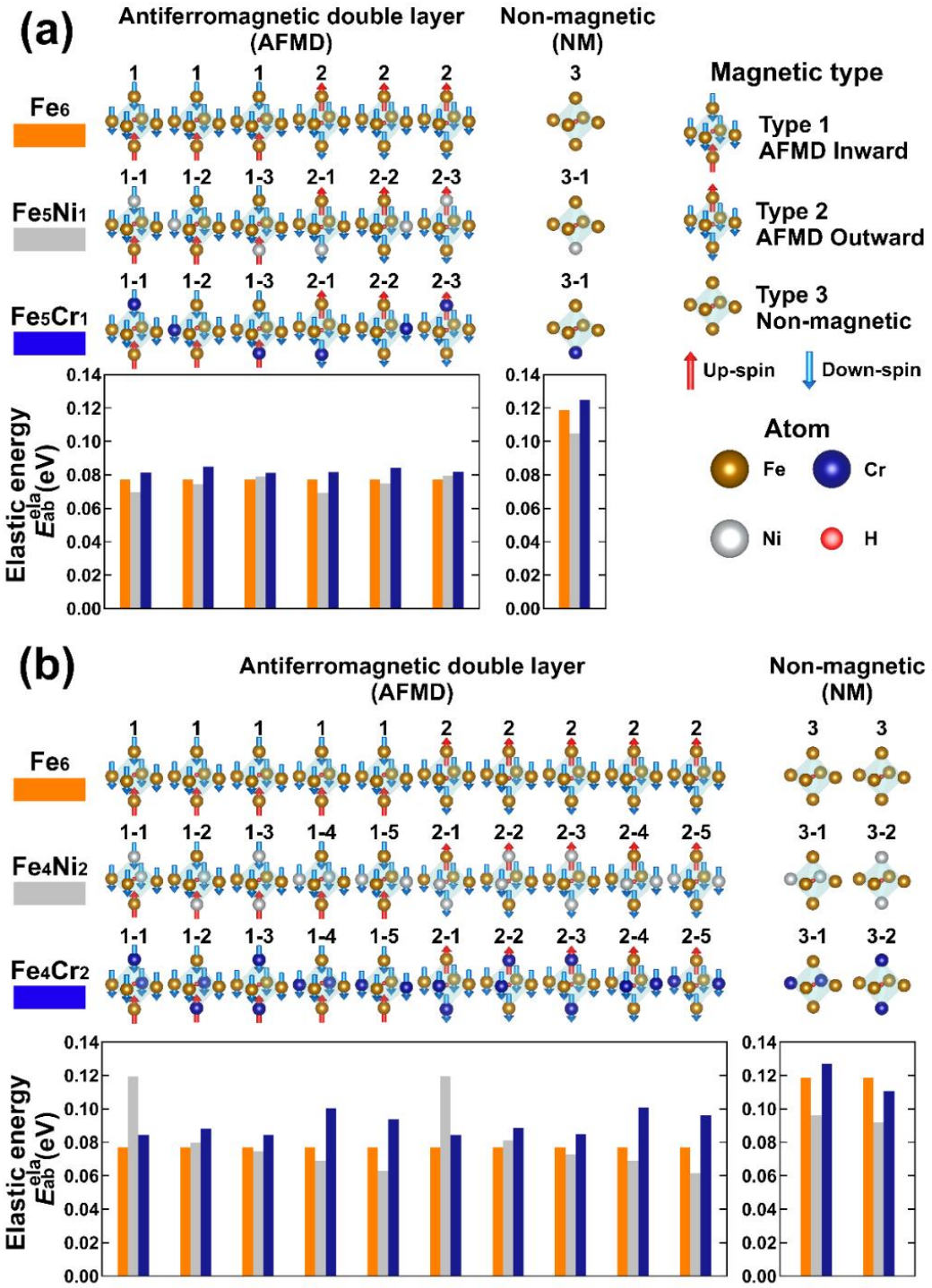

295 **Fig. 4**. The elastic energy, E_{ab}^{ela}, at O-sites of (a) $Fe_{31}X_1$ (X: Fe, Ni, Cr) (b) $Fe_{30}X_2$ (X: Fe, Ni,
296 Cr) in the AFMD and NM states. Up and down arrows in the AFMD state represent up- and
297 down-spin.

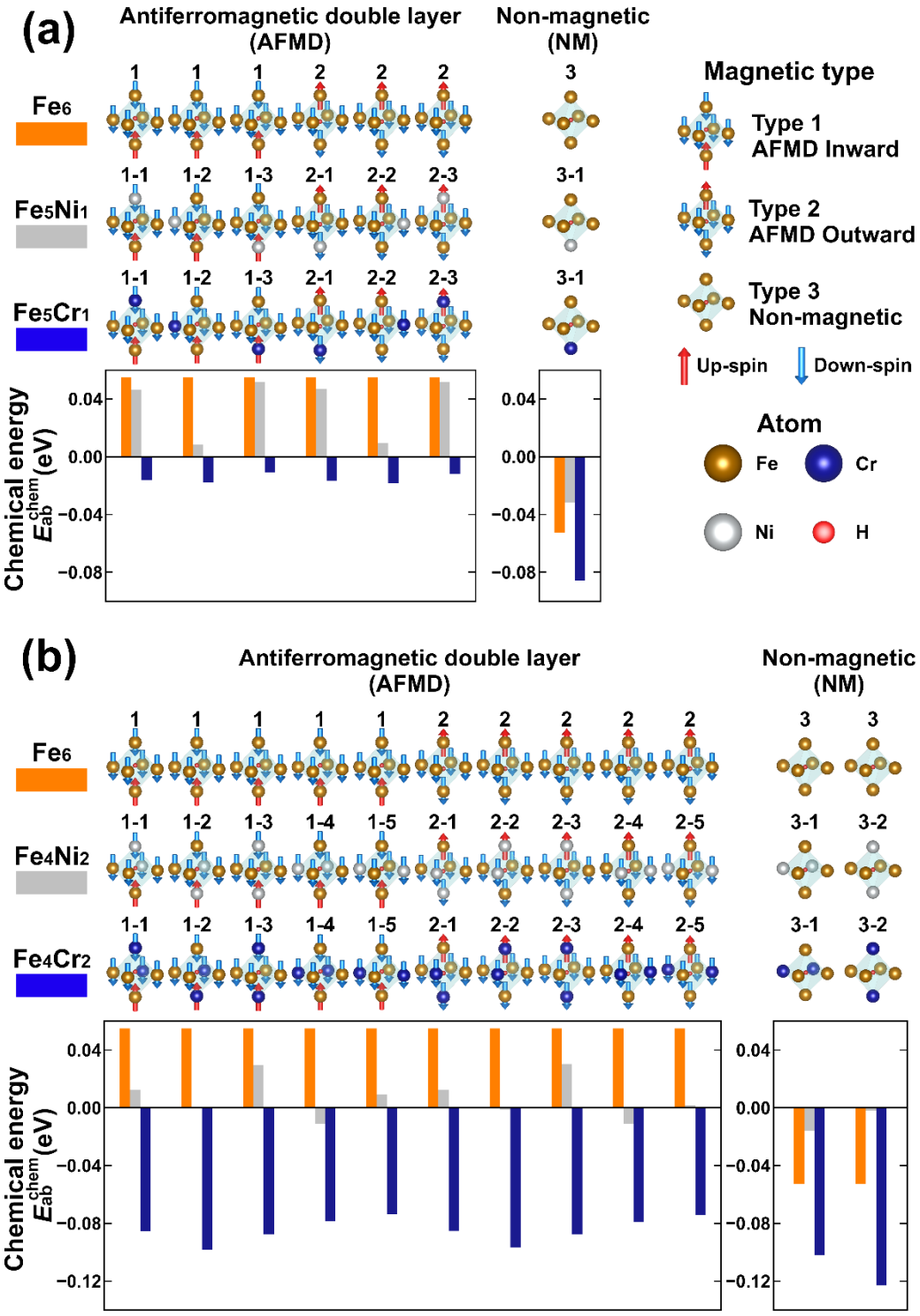

Fig. 5. The chemical energy, E_{ab}^{chem}, at O-sites of (a) $Fe_{31}X_1$ (X: Fe, Ni, Cr) (b) $Fe_{30}X_2$ (X: Fe, Ni, Cr) in the AFMD and NM states. Up and down arrows in the AFMD state represent up- and down-spin.

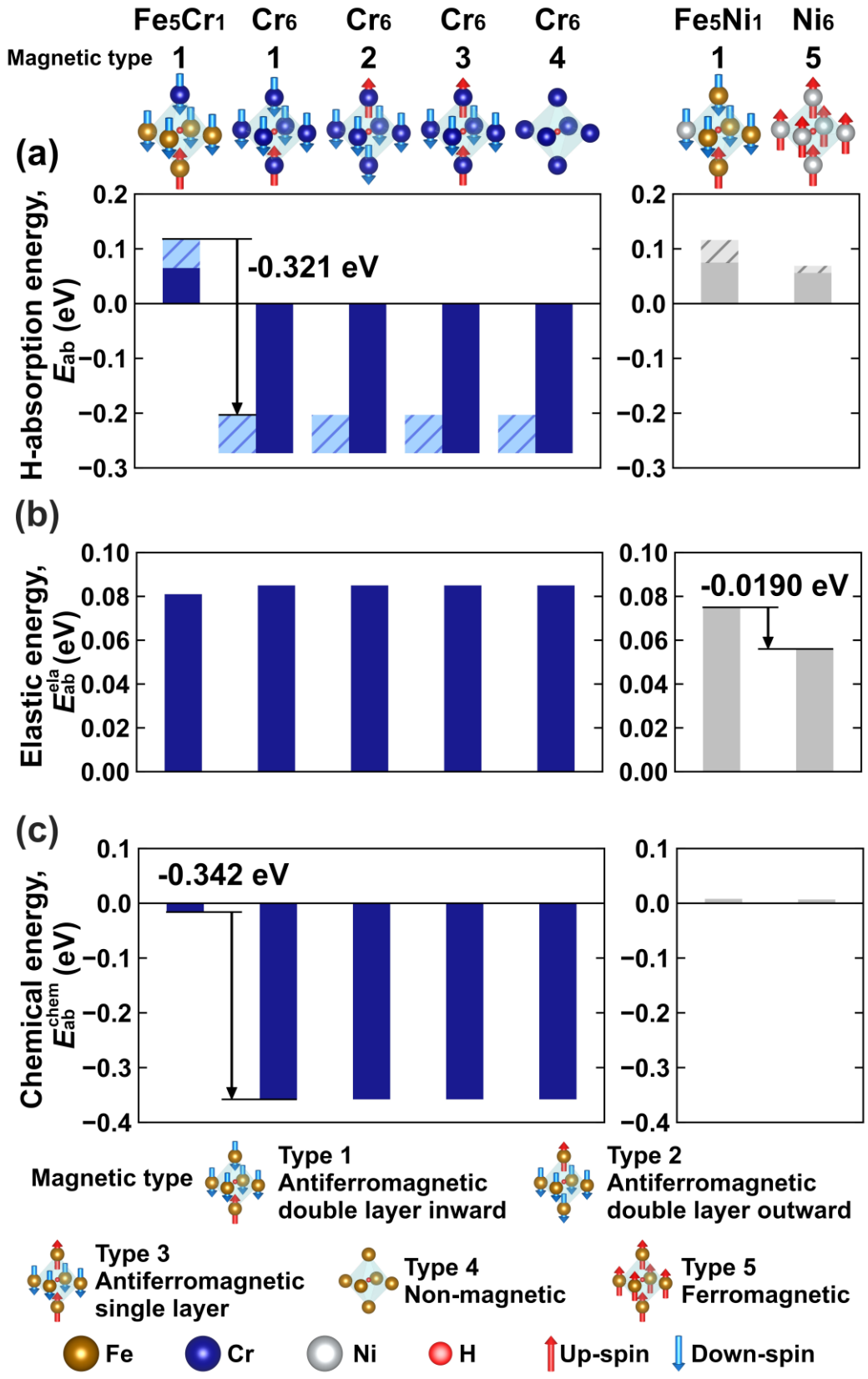

303 **Fig. 6**. The difference between the contribution of Cr and Ni to the H-absorption energy at the
304 O-site for Fe_5Cr_1 in $Fe_{31}Cr_1$ cell, Cr_6 in Cr_{32} cell, Fe_5Ni_1 in $Fe_{31}Ni_1$ cell, and Ni_6 in Ni_{32} cell. (a)

H-absorption energy, E_{ab}. The part of zero-point energy correction, E_{ZP}, is represented as shown as bars filled with a hatched pattern. (b) Elastic energy, E_{ab}^{ela}, (c) chemical energy, E_{ab}^{chem}. Up and down arrows represent up- and down-spin.

4. H-occupancy calculated by H-absorption energy

4.1 Mean H-absorption energy of the O-sites in Fe-Cr-Ni-based austenitic alloys with any chemical composition

Figure 7 shows the correlation between the H-absorption energy, E_{ab}, described in Figs. 2 and 6 and the number of Cr and Ni atoms in the O-sites. Please Note that the E_{ab} in Fig. 7 is the average value of the various O-site patterns generated by the different locations of substitution atoms and magnetic moment shown in Figs. 2 and 6. Assuming that E_{ab} changes linearly with the number of Cr and Ni atoms, E_{ab} at the O-sites in Fe-Cr and Fe-Ni systems is given by the following equations.

$$E_{ab} = 0.186 - 0.0646n_{Cr} \quad (8)$$

$$E_{ab} = 0.186 - 0.0178n_{Ni} \quad (9)$$

n_{Cr} and n_{Ni} are the numbers of Cr and Ni atoms in the O-sites, and 0.186 eV is the E_{ab} at the O-sites consisting of Fe atoms only.

We predicted the H-occupancy, θ_L, of the various Fe-Cr-Ni-based austenitic alloys by the H-absorption energy at the O-sites. Neglecting the interaction between Cr and Ni atoms constituting the same O-site, E_{ab} is roughly described by the following equation.

$$E_{ab} = 0.186 - 0.0646n_{Cr} - 0.0178n_{Ni} \quad (10)$$

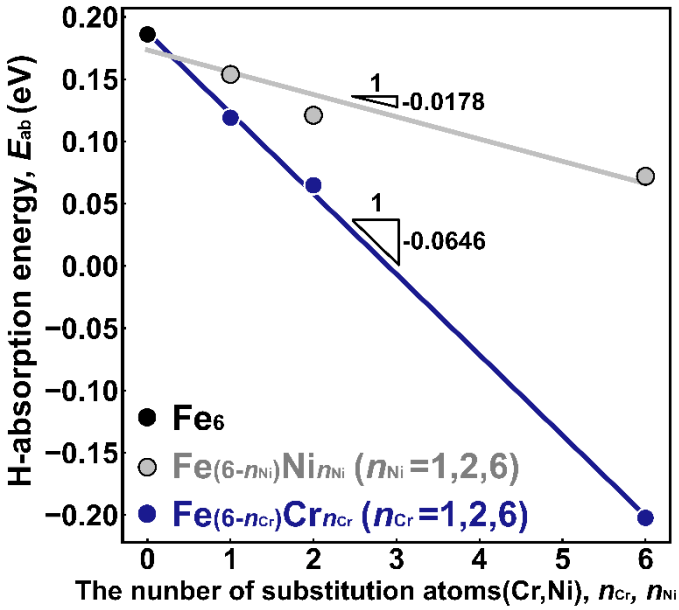

Fig. 7. Variation in the mean H-absorption energy, E_{ab}, at O-sites under AFMD as a function of the number of Cr atoms, n_{Cr}, and Ni atoms, n_{Ni}. When n_{Cr} and n_{Ni} = 1, each value of E_{ab} in Fig. 7 is the average value of E_{ab} of the O-site patterns under AFMD shown in Fig. 2 (a), i.e., n_{Cr} and n_{Ni} = 2 in Fig. 2 (b), and n_{Cr} and n_{Ni} = 6 in Fig. 6 (a).

4.2 H-occupancy in alloys with various atomic ratios of alloying elements

To calculate the H-occupancy θ_L of Fe-Cr-Ni-based austenitic alloys with various atomic ratio, we generated 100,000 random combinations of six atoms consisting of the O-sites along with the atomic ratio of each alloy, and calculated each E_{ab} using Eq. (10) in Section 4.1. The θ_L of each alloy is the average of H-occupancies from each E_{ab} according to Eq. (5) in Section 2.5.

Figure 8 shows the H-occupancy θ_L with an arbitrary atomic ratio, derived using the above method, together with the experimental results in Table 2. The θ_L values were sorted in ascending order by the sum of the atomic Cr and Ni ratio in Table 2. Over the wide range of totals of Cr and Ni ratios (0 – 36.0 at %), e.g., 16Cr-10Ni to 22Cr-12Ni in Fig. 8, the θ_L values in the present study are closely consistent with the experimental results for the absolute value. In contrast, when the sum of Cr and Ni ratio exceeds 36.0 at %, as represented by 23Cr-13Ni to 18Cr-35Ni, the calculated result is higher than the experimental one, although the patterns are the same.

To examine the above discrepancies between the experimental and calculated values for H-occupancy θ_L, Fig. 9 shows the relationship between the discrepancy and (a) the totals of the Cr and Ni atomic ratios, (b) the Cr atomic ratio, and (c) the Ni atomic ratio. The discrepancy became more marked as the totals of the Cr and Ni atomic ratios increased. Specifically, the H-absorption energy E_{ab} derived from Eq. (11) was increasingly underestimated with rising totals of Cr and Ni content. Figures 9 (b) and (c) show that the discrepancy did not correlate with Cr content: it appears to be a function of Ni, except for 0Cr-36Ni. It was more pronounced in 18Cr-35Ni than in 0Cr-36Ni, even with a similar Ni content. Thus, interaction between Cr and Ni atoms is significant if the Fe-Cr-Ni-based austenitic alloy contains a high amount of Cr and Ni, e.g., the sum value exceeds 36.0 at%. Although the interaction between Cr and Ni has been well reported, the interaction between certain alloying elemenets has been studied from the perspective of the phase stability of Nb-Si alloy [40]. The Zr and Hf atoms reduced the stability of the Nb phase in the alloy. Only when another atom (Al, Ni) was contained in the Nb phase, Zr and Hf atoms stabilized the Nb phase dur to the synergetic effect with Al and Ni atoms. Therefore, there is a possibility that the Cr and Ni atoms have such a synergetic effect on the H-absorption energy.

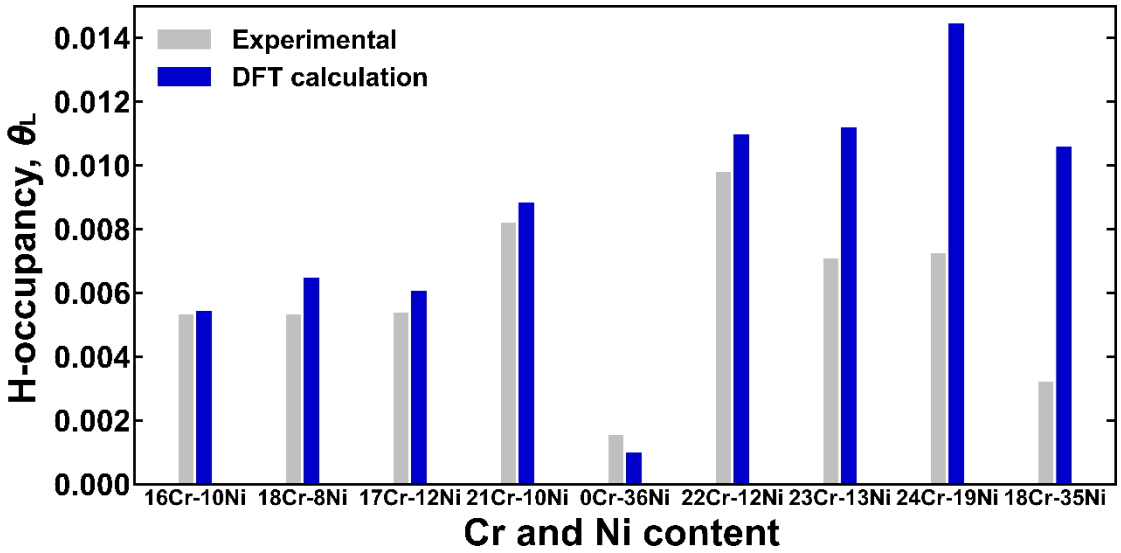

Fig. 8. H-occupancy θ_L of Fe-Cr-Ni-based austenitic alloys with various Cr and Ni contents obtained by DFT calculations in the present study and experiments in past studies [18,38].

Table 2. Overall data of the H-occupancy, the Cr-equivalent in the various Fe-Cr-Ni-based austenitic alloys, generated by the experiments and DFT calculations, together with the discrepancy between the DFT and experiments[18,38].

Materials	mass Cr %	mass Ni %	atomic Cr	atomic Ni	H-occupancy ($\times 10^{-3}$) in Fig. 8		Discrepancy % in Fig. 9	Cr-equivalent in Fig. 10
					Experiments	DFT calculation		
16Cr-10Ni (AISI 316)	16.2	10.1	0.172	0.0958	5.32	5.35	0.612	0.199
18Cr-8Ni (AISI 304)	18.2	8.18	0.193	0.0770	5.32	6.46	21.4	0.214
17Cr-12Ni (AISI 316L)	16.8	12.1	0.179	0.114	5.37	5.92	10.2	0.210
21Cr-10Ni (HPI 160)	20.7	9.71	0.219	0.0914	8.37	8.74	6.58	0.245
0Cr-36Ni (UNS K93600)	0.00	36.1	0.00	0.349	1.52	0.975	-35.8	0.0963
22Cr-12Ni (XM 19)	22.4	12.5	0.238	0.117	9.77	10.8	11.1	0.270
23Cr-13Ni (AISI 309S)	22.5	13.3	0.239	0.125	7.06	11.2	58.6	0.274

24Cr-19Ni (AISI 310S)	24.2	19.1	0.257	0.179	7.22	14.4	99.9	0.307
18Cr-35Ni (UNS K08330)	18.4	35.1	0.198	0.335	3.20	10.4	227	0.290

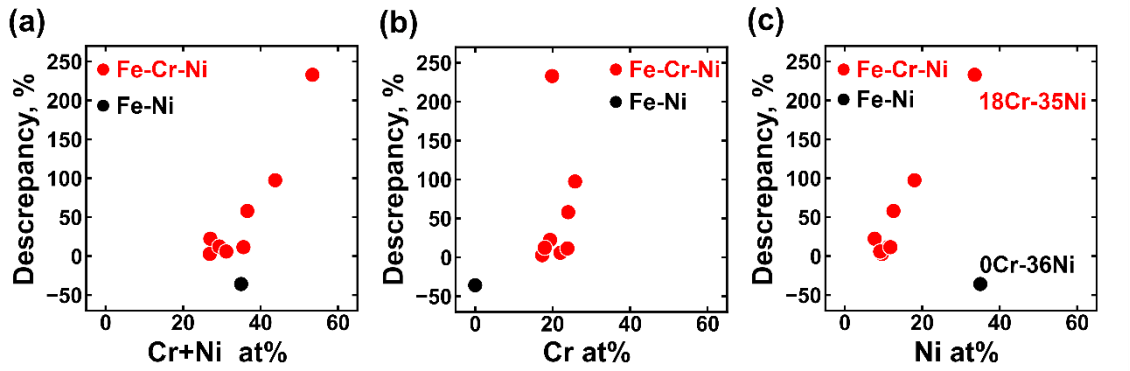

Fig. 9. The discrepancy between the H-occupancy θ_L of Fe-Cr-Ni-based austenitic alloys with various Cr and Ni content obtained by DFT calculations and experiments in past studies [18,38] in Table 2 versus (a) the totals of the Cr and Ni atomic ratios, (b) the Cr atomic ratio, and (c) the Ni atomic ratio.

As shown in Fig. 8, the H-occupancy of Fe-Cr-Ni-based austenitic alloys can be estimated by the H-absorption energy when the total Cr and Ni content is below 36.0 at%, without taking into account the interaction between Cr and Ni. As an index of H-occupancy of Fe-Cr-Ni-based austenitic alloys, we propose the Cr-equivalent, $Cr_{eq\text{-}H}$, as follows.

$$Cr_{eq\text{-}H}=1[\mathrm{Cr}]+0.276[\mathrm{Ni}] \quad (11)$$

$[\mathrm{Cr}]$ and $[\mathrm{Ni}]$ denote the Cr and Ni atomic ratios. The coefficient of 0.276 represents the contribution of Ni to the H-absorption energy based on that of Cr, i.e., 0.0178 / 0.0646. Figure 10 plots the experimentally-derived H-occupancies [18,38] and the calculated H-occupancies in the present study as a function of $Cr_{eq\text{-}H}$. The calculated H-occupancies were closely consistent with the results of experiments in the range $Cr_{eq\text{-}H} < 0.250$. The $Cr_{eq\text{-}H}$ influences the H content derived from the change in the H-absorption energy in the Fe-Cr-Ni sytem. Consequently, the higher the H content, i.e., the lower the H-absorption energy, the greater the improvement in the strength and ductility balance in the Fe-Cr-Ni alloy. Although H-occupancy is overestimated in the range of $Cr_{eq\text{-}H}$ greater than 0.250, $Cr_{eq\text{-}H}$ can be used as an index of the H-occupancy of Fe-Cr-Ni-based austenitic alloys when $Cr_{eq\text{-}H} < 0.250$. The interaction between Cr and Ni atoms should be incorporated such that $Cr_{eq\text{-}H}$ can estimate the H-occupancy accurately without any limitations on Cr and Ni content.

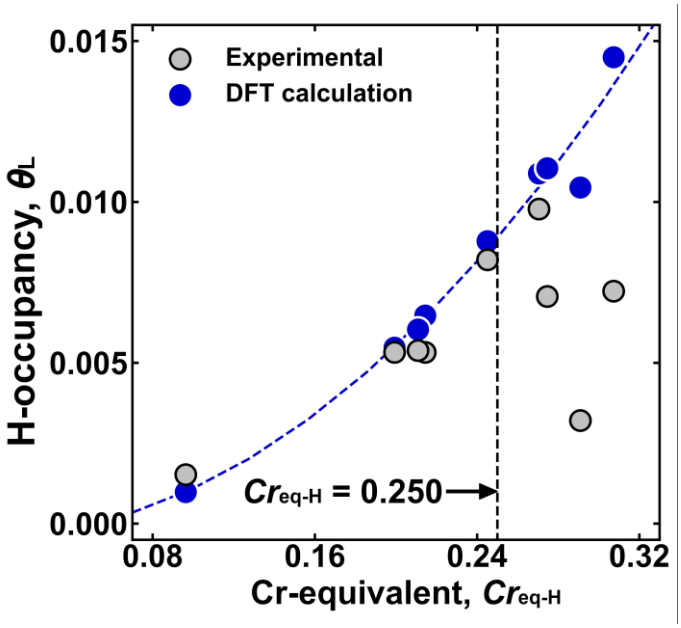

Fig. 10. The H-occupancy θ_L of Fe-Cr-Ni-based austenitic alloys with various Cr and Ni contents obtained by DFT calculations and experiments in past studies [18,38] versus the Cr-equivalent, $Cr_{eq\text{-}H}$ in Table 2.

5. Conclusions

To understand the details of various dissolved H content in Fe-Cr-Ni-based austenitic alloys as a function of the alloying elements, we investigated the effects of Cr and Ni on H-absorption energy at O-sites by employing DFT calculations in AFMD and NM states. The H-occupancy calculated based on H-absorption energy was directly compared with the experimental results for various Fe-Cr-Ni-based austenitic alloys. The primary insights are summarized as follows.

(1) Replacing Fe with Cr and Ni reduces the H-absorption energy, i.e., increases the H-occupancy. This reduction becomes more pronounced with substitutions by Cr than by Ni.

(2) The reduction in the H-absorption energy stems primarily from a decrease in chemical energy rather than a decrease in elastic energy. Chromium reduces the chemical energy in H-absorption to a substantially greater degree than does Ni.

(3) The H-absorption energy E_{ab} at the O-sites in the Fe-Cr-Ni austenitic alloy system is given as follows.

$$E_{\mathrm{ab}} = 0.186 - 0.0646n_{\mathrm{Cr}} - 0.0178n_{\mathrm{Ni}}$$

The calculated H-occupancy by E_{ab} strongly supports the experimental results as absolute values over a wide range of totaled Cr and Ni content (< 36.0 at%). When it exceeds 36.0 at%, the calculated H-occupancy is overestimated compared to the experimental results, likely due to the calculation not including the effects on H-absorption energy of interactions between Cr and Ni atoms.

(4) The Cr-equivalent $Cr_{\mathrm{eq\text{-}H}}$ is thus a potentially useful index of H-occupancy of Fe-Cr-Ni-based austenitic alloys when $Cr_{\mathrm{eq\text{-}H}}$ < 0.250. When $Cr_{\mathrm{eq\text{-}H}}$ > 0.250, a divergence is generated between the calculated and experimental results due to interactions between the Cr and Ni atoms.

Acknowledgments

This study was partly supported by JSPS KAKENHI (JP20K04161; JP21K04702; JP21K14045) and the Yoshida Gakujutsu Foundation. The authors are grateful to Prof. Hiroyuki Toda at Kyushu University for his helpful comments on Section 4.3.

Reference

[1] T. Michler, C. San Marchi, J. Naumann, S. Weber, M. Martin, Hydrogen environment embrittlement of stable austenitic steels, Int. J. Hydrogen Energy. 37 (2012) 16231–16246. https://doi.org/10.1016/j.ijhydene.2012.08.071.

[2] S. Matsuoka, J. Yamabe, H. Matsunaga, Criteria for determining hydrogen compatibility and the mechanisms for hydrogen-assisted, surface crack growth in austenitic stainless steels, Eng. Fract. Mech. 153 (2016) 103–127. https://doi.org/10.1016/j.engfracmech.2015.12.023.

[3] K.A. Nibur, B.P. Somerday, C.S. Marchi, J.W. Foulk, M. Dadfarnia, P. Sofronis, The Relationship Between Crack-Tip Strain and Subcritical Cracking Thresholds for Steels in High-Pressure Hydrogen Gas, Metall. Mater. Trans. A. 44 (2013) 248–269. https://doi.org/10.1007/s11661-012-1400-5.

[4] J.P. Hirth, Effects of hydrogen on the properties of iron and steel, Metall. Trans. A. 11 (1980) 861–890. https://doi.org/10.1007/BF02654700.

[5] M. Wang, E. Akiyama, K. Tsuzaki, Effect of hydrogen on the fracture behavior of high strength steel during slow strain rate test, Corros. Sci. 49 (2007) 4081–4097. https://doi.org/10.1016/J.CORSCI.2007.03.038.

[6] L. Zhang, B. An, S. Fukuyama, T. Iijima, K. Yokogawa, Characterization of hydrogen-induced crack initiation in metastable austenitic stainless steels during deformation, J. Appl. Phys. 108 (2010) 063526. https://doi.org/10.1063/1.3477321.

[7] M. Koyama, T. Ogawa, D. Yan, Y. Matsumoto, C.C. Tasan, K. Takai, K. Tsuzaki, Hydrogen desorption and cracking associated with martensitic transformation in Fe-Cr-Ni-Based austenitic steels with different carbon contents, Int. J. Hydrogen Energy. 42 (2017) 26423–26435. https://doi.org/10.1016/j.ijhydene.2017.08.209.
[8] L. Zhang, M. Wen, M. Imade, S. Fukuyama, K. Yokogawa, Effect of nickel equivalent on hydrogen gas embrittlement of austenitic stainless steels based on type 316 at low temperatures, Acta Mater. 56 (2008) 3414–3421. https://doi.org/10.1016/J.ACTAMAT.2008.03.022.
[9] G. Han, S. He, S. Fukuyama, K. Yokogawa, Effect of Nickel Equivalent on Hydrogen Environment Embrittlement of Austenitc Stainless Steels at Low Temperatures, Acta Mater. 46 (1998) 4599–4570.
[10] T. Omura, J. Nakamura, H. Hirata, K. Jotoku, M. Ueyama, T. Osuki, M. Terunuma, Effect of Surface Hydrogen Concentration on Hydrogen Embrittlement Properties of Stainless Steels and Ni Based Alloys, ISIJ Int. 56 (2016) 405–412. https://doi.org/10.2355/isijinternational.ISIJINT-2015-268.
[11] T. Boniszewski, G.C. Smith, The influence of hydrogen on the plastic deformation ductility, and fracture of nickel in tension, Acta Metall. 11 (1963) 165–178. https://doi.org/10.1016/0001-6160(63)90209-8.
[12] Z.D. Harris, S.K. Lawrence, D.L. Medlin, G. Guetard, J.T. Burns, B.P. Somerday, Elucidating the contribution of mobile hydrogen-deformation interactions to hydrogen-induced intergranular cracking in polycrystalline nickel, Acta Mater. 158 (2018) 180–192. https://doi.org/10.1016/j.actamat.2018.07.043.
[13] K. Wada, J. Yamabe, Y. Ogawa, O. Takakuwa, T. Iijima, H. Matsunaga, Comparative study of hydrogen-induced intergranular fracture behavior in Ni and Cu–Ni alloy at ambient and cryogenic temperatures, Mater. Sci. Eng. A. 766 (2019) 138349. https://doi.org/10.1016/j.msea.2019.138349.
[14] D.P. Abraham, C.J. Altstetter, The effect of hydrogen on the yield and flow stress of an austenitic stainless steel, Metall. Mater. Trans. A. 26 (1995) 2849–2858. https://doi.org/10.1007/BF02669643.
[15] K. Yamada, M. Koyama, K. Tsuzaki, Positive and negative effects of hydrogen on tensile behavior in polycrystalline Fe – 30Mn –(6 À x) Si – x Al austenitic alloys, Scr. Mater. 105 (2015) 54–57. https://doi.org/10.1016/j.scriptamat.2015.05.007.
[16] H. Luo, Z. Li, D. Raabe, Hydrogen enhances strength and ductility of an equiatomic high-entropy alloy, Sci. Rep. 7 (2017) 1–7. https://doi.org/10.1038/s41598-017-10774-4.
[17] Y. Ogawa, H. Hosoi, K. Tsuzaki, T. Redarce, O. Takakuwa, H. Matsunaga, Hydrogen, as an alloying element, enables a greater strength-ductility balance in an Fe-Cr-Ni-based, stable austenitic stainless steel, Acta Mater. 199 (2020) 181–192. https://doi.org/10.1016/j.actamat.2020.08.024.
[18] H. Nishida, Y. Ogawa, K. Tsuzaki, Chemical composition dependence of the strength and ductility enhancement by solute hydrogen in Fe–Cr–Ni-based austenitic alloys, Mater. Sci. Eng. A. 836 (2022) 142681. https://doi.org/10.1016/j.msea.2022.142681.
[19] X. Zhou, W.A. Curtin, First principles study of the effect of hydrogen in austenitic stainless steels and high entropy alloys, Acta Mater. 200 (2020) 932–

942. https://doi.org/10.1016/j.actamat.2020.09.070.
[20] L. Ismer, T. Hickel, J. Neugebauer, Ab initio study of the solubility and kinetics of hydrogen in austenitic high Mn steels, Phys. Rev. B - Condens. Matter Mater. Phys. 81 (2010) 20–23. https://doi.org/10.1103/PhysRevB.81.094111.
[21] V. Appen, R. Dronskowski, A. Chakrabarty, T. Hickel, Impact of Mn on the Solution Enthalpy of Hydrogen in Austenitic Fe-Mn Alloys : A First-Principles Study, (2014) 2239–2244. https://doi.org/10.1002/jcc.23742.
[22] E.J. Song, H.K.D.H. Bhadeshia, D.-W. Suh, Interaction of aluminium with hydrogen in twinning-induced plasticity steel, Scr. Mater. 87 (2014) 9–12. https://doi.org/10.1016/j.scriptamat.2014.06.007.
[23] G. Kresse, J. Hafner, Ab initio molecular dynamics for open-shell transition metals, Phys. Rev. B. 48 (1993) 13115–13118. https://doi.org/10.1103/PhysRevB.48.13115.
[24] G. Kresse, J. Furthmüller, Efficient iterative schemes for ab initio total-energy calculations using a plane-wave basis set, Phys. Rev. B - Condens. Matter Mater. Phys. 54 (1996) 11169–11186. https://doi.org/10.1103/PhysRevB.54.11169.
[25] G. Kresse, J. Furthmüller, Efficiency of ab-initio total energy calculations for metals and semiconductors using a plane-wave basis set, Comput. Mater. Sci. 6 (1996) 15–50. https://doi.org/10.1016/0927-0256(96)00008-0.
[26] J.P. Perdew, K. Burke, M. Ernzerhof, Generalized Gradient Approximation Made Simple, (1996) 3865–3868.
[27] P.E. Blöchl, Projector augmented-wave method, Phys. Rev. B. 50 (1994) 17953–17979. https://doi.org/10.1103/PhysRevB.50.17953.
[28] M. Methfessel, A.T. Paxton, High-precision sampling for Brillouin-zone integration in metals, Phys. Rev. B. 40 (1989) 3616–3621. https://doi.org/10.1103/PhysRevB.40.3616.
[29] H.J. Monkhorst, J.D. Pack, Special points for Brillouin-zone integrations, Phys. Rev. B. 13 (1976) 5188–5192. https://doi.org/10.1103/PhysRevB.13.5188.
[30] K. Momma, F. Izumi, VESTA 3 for three-dimensional visualization of crystal, volumetric and morphology data, J. Appl. Crystallogr. 44 (2011) 1272–1276. https://doi.org/10.1107/S0021889811038970.
[31] H.C. Herper, E. Hoffmann, P. Entel, Ab initio full-potential study of the structural and magnetic phase stability of iron, Phys. Rev. B - Condens. Matter Mater. Phys. 60 (1999) 3839–3848. https://doi.org/10.1103/PhysRevB.60.3839.
[32] D. Qian, X.F. Jin, Spin-Density Wave in Ultrathin Fe Films on Cu (100), (2001) 1–4. https://doi.org/10.1103/PhysRevLett.87.227204.
[33] I.A. Abrikosov, A.E. Kissavos, F. Liot, B. Alling, S.I. Simak, O. Peil, A. V. Ruban, Competition between magnetic structures in the Fe rich fcc FeNi alloys, Phys. Rev. B - Condens. Matter Mater. Phys. 76 (2007) 1–14. https://doi.org/10.1103/PhysRevB.76.014434.
[34] R. Nazarov, T. Hickel, J. Neugebauer, First-principles study of the thermodynamics of hydrogen-vacancy interaction in fcc iron, (2010) 1–11. https://doi.org/10.1103/PhysRevB.82.224104.
[35] H. Sugimoto, Y. Fukai, Solubility of hydrogen in metals under high hydrogen pressures: Thermodynamical calculations, Acta Metall. Mater. 40 (1992) 2327–2336. https://doi.org/10.1016/0956-7151(92)90151-4.
[36] J.S. Wróbel, D. Nguyen-Manh, M.Y. Lavrentiev, M. Muzyk, S.L. Dudarev,

Phase stability of ternary fcc and bcc Fe-Cr-Ni alloys, Phys. Rev. B. 91 (2015) 024108. https://doi.org/10.1103/PhysRevB.91.024108.
[37] C.S. Marchi, B.P. Somerday, R.S. Larson, S.F. Rice, Solubility of hydrogen and its isotopes in metals from mixed gases, 372 (2008) 421–425. https://doi.org/10.1016/j.jnucmat.2007.02.016.
[38] J. Yamabe, O. Takakuwa, H. Matsunaga, H. Itoga, S. Matsuoka, Hydrogen diffusivity and tensile-ductility loss of solution-treated austenitic stainless steels with external and internal hydrogen, Int. J. Hydrogen Energy. 42 (2017) 13289–13299. https://doi.org/10.1016/j.ijhydene.2017.04.055.
[39] A. Machida, H. Saitoh, H. Sugimoto, T. Hattori, A. Sano-Furukawa, N. Endo, Y. Katayama, R. Iizuka, T. Sato, M. Matsuo, S.I. Orimo, K. Aoki, Site occupancy of interstitial deuterium atoms in face-centred cubic iron, Nat. Commun. 5 (2014) 2–5. https://doi.org/10.1038/ncomms6063.
[40] Y. Tang, B. Xiao, J. Chen, F. Liu, W. Du, J. Guo, Y. Liu, Y. Liu, Multi-component Alloying Effects on the Stability and Mechanical Properties of Nb and Nb–Si Alloys: A First-Principles Study, Metall. Mater. Trans. A. 54 (2023) 450–472. https://doi.org/10.1007/s11661-022-06868-y.